

Overview of the $(g - 2)_\mu$ status and related e^+e^- measurements in Novosibirsk and by ISR

V. P. Druzhinin*

Budker Institute of Nuclear Physics, Novosibirsk, 630090, Russia

Novosibirsk State University, Novosibirsk, 630090, Russia

E-mail: druzhinin@inp.nsk.su

Recent measurements of exclusive hadronic cross sections in e^+e^- experiments important for calculation of the leading-order hadronic contribution to the muon anomalous magnetic moment are reviewed.

The 15th International Conference on Flavor Physics & CP Violation

5-9 June 2017

Prague, Czech Republic

*Speaker.

QED	11658471.895	± 0.008
LO hadronic vacuum polarization	693.1	± 3.4
NLO+NNLO hadronic vacuum polarization	-8.63	± 0.09
Hadronic light-by-light	10.5	± 2.6
Electroweak	15.4	± 0.1
Theory	11659182.3	± 4.3
Experiment (E821@BNL)	11659209.1	± 6.3
Experiment – Theory	26.8	± 7.6

Table 1: Contributions to the SM prediction for a_μ (10^{-10}) [4] and comparison with experiment [1].

1. Introduction

The magnetic moment of a particle is expressed in terms of the g -factor:

$$\vec{\mu} = g \frac{e\hbar}{2mc} \vec{S}, \quad (1.1)$$

where e , m , and \vec{S} are the particle charge, mass, and spin. The Dirac equation predicts $g = 2$ for point-like fermions. Higher order radiative corrections lead to deviation from 2. The anomalous magnetic moment for muon is defined as $a_\mu = (g_\mu - 2)/2$. The examples of diagrams describing pure QED, hadronic, and weak contributions into the anomalous magnetic moment are shown in Fig. 1. Since all possible particles can contribute to a_μ via loops, its value is sensitive to new physics beyond the Standard Model (SM).

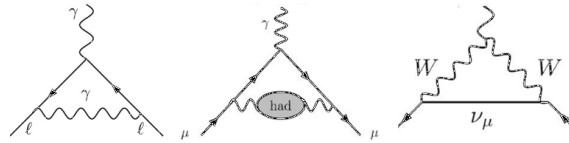


Figure 1: Examples of diagrams describing QED (left), hadronic (middle), and weak (right) contributions into the anomalous magnetic moment.

The anomalous magnetic moment of the muon was measured in the Brookhaven's E-821 experiment with accuracy of about 0.5 ppm [1]. Two new experiments are planned, at Fermilab [2] and J-PARC [3], which will improve accuracy by a factor of at least 4.

The a_μ value is precisely predicted theoretically within the framework of the Standard Model. The different SM contributions to a_μ taken from Ref. [4] are listed in Table 1. The largest contribution comes from QED. The next largest is a leading order (LO) hadronic vacuum polarization contribution ($a_\mu^{\text{had, LO}}$), which determines more than 50% of the error of the a_μ SM prediction. Currently, about 3.5σ difference is observed between experiment and the SM calculation (see also Ref. [5], where this difference is found to be 4.1σ).

The leading-order hadronic contribution coming from hadron loops (Fig. 1 (middle)) cannot be calculated accurately from theory alone. It is calculated using dispersion relation from experimental measurements of the total cross section e^+e^- annihilation into hadrons. Low energies, below 2

GeV, give dominant contribution into $a_\mu^{\text{had, LO}}$. In this energy region the total hadronic cross section is calculated as a sum of exclusive hadronic cross sections.

Two experimental techniques are used to measure hadronic cross sections. The conventional method is the energy scan. Currently operating machines using this method are VEPP-2000 below 2 GeV, and VEPP-4M and BEPCII above. The initial state radiation (ISR) technique for measurement of exclusive cross sections is used in the KLOE, BESIII, and BABAR experiments.

In next sections we will discuss recent results on measurements of exclusive hadronic cross sections at low energies.

2. e⁺e⁻ → π⁺π⁻

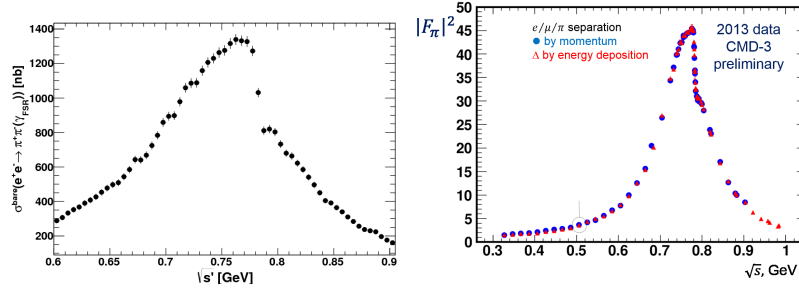


Figure 2: The $e^+e^- \rightarrow \pi^+\pi^-$ cross section measured in the BESIII (left) and CMD-3 (right) experiments.

The main contribution into the hadronic part of a_μ and its error comes from $e^+e^- \rightarrow \pi^+\pi^-$ process. The many experiments measured this cross section especially in the ρ meson energy region. Most precise and complete scan measurement is performed by CMD-2 at VEPP-2M [6] in the energy region from 0.37 to 1.38 GeV. During the last decade, large progress was reached in ISR measurements, in the KLOE [7], BABAR [8], and BESIII [9] experiments. The CMD-2, KLOE, BABAR, and BESIII claim systematic uncertainties at a sub-percent level. The $e^+e^- \rightarrow \pi^+\pi^-$ cross section measured by BESIII [9] is shown in Fig. 2 (left).

Currently the accuracy of the $\pi\pi$ contribution into a_μ is estimated to be about 0.5% [4] and dominated by systematic uncertainty. The problem of the $\pi^+\pi^-$ measurements is that the systematic differences between cross-section data from different experiments (see Ref. [9]) reach 5% and significantly exceed claimed systematic uncertainties (<1%).

The existing scan $e^+e^- \rightarrow \pi^+\pi^-$ measurements have large statistical errors. The VEPP-2000 collider allows to significantly increase statistics and made scan measurements comparable in accuracy with ISR data. In Fig. 2 (right) the preliminary result of the CMD-3 experiment based on data collected at VEPP-2000 in 2013 is shown. Two methods of $e/\pi/\mu$ separation, by momentum and by energy deposition in the calorimeter, are used to estimate systematic uncertainty due to particle identification. The statistical accuracy of this measurement matches or better the current world-best. For 2013 data, CMD-3 expects to reach a systematic uncertainty of below 1%.

3. e⁺e⁻ → π⁺π⁻π⁰π⁰

The $e^+e^- \rightarrow \pi^+\pi^-\pi^0\pi^0$ cross section is one of the least known cross section important for

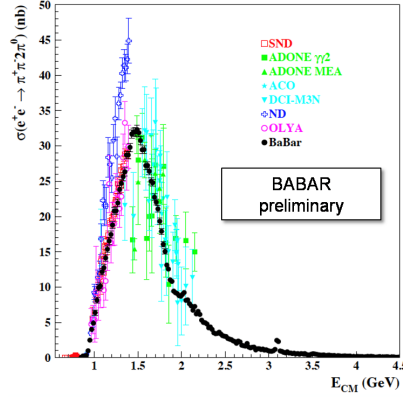


Figure 3: The $e^+e^- \rightarrow \pi^+\pi^-2\pi^0$ cross section measured by BABAR in comparison with previous measurements. The quoted errors are statistical.

$(g-2)_\mu$.

The preliminary BABAR result on the $e^+e^- \rightarrow \pi^+\pi^-2\pi^0$ cross section in comparison with previous measurements is shown in Fig. 3, The BABAR measurements are most precise, especially above 1.4 GeV, and covers a wider energy region. Their systematic uncertainty is 3.1% in the energy region between 1.2 and 2.7 GeV.

The obtained cross section data are used to calculate the $e^+e^- \rightarrow \pi^+\pi^-2\pi^0$ contribution to $a_\mu^{\text{had, LO}}$. For the energy region below 1.8 GeV it is equal to $(17.9 \pm 0.1_{\text{stat}} \pm 0.6_{\text{syst}}) \times 10^{-10}$. This result can be compared with the previous calculation [10] based on the preliminary BABAR data on $e^+e^- \rightarrow \pi^+\pi^-2\pi^0$ from 2007 [11]: $(18.0 \pm 0.1_{\text{stat}} \pm 1.2_{\text{syst}}) \times 10^{-10}$. The new BABAR measurement improves accuracy of this contribution by a factor of 2.

4. $e^+e^- \rightarrow \pi^0\gamma$

The $e^+e^- \rightarrow \pi^0\gamma$ cross section is the third largest cross section (after $e^+e^- \rightarrow \pi^+\pi^-$ and $\pi^+\pi^-\pi^0$) below 1 GeV. From analysis of the $e^+e^- \rightarrow \pi^0\gamma$ data in the vector meson dominance (VMD) model, the widths of vector-meson radiative decays are extracted, which are widely used in phenomenological models.

The precise measurement of the $e^+e^- \rightarrow \pi^0\gamma$ cross section was recently performed by the SND detector using the full data set collected at the VEPP-2M e^+e^- collider in 1997-2000 [12]. The result of this measurement is shown in Fig. 4 in five energy regions in comparison with previous measurements. The systematic uncertainty in the cross section maximum at ω peak is 1.4%. In the highest energy region, the preliminary SND result based on VEPP-2000 data is shown.

5. $e^+e^- \rightarrow K\bar{K}$

The largest contribution to $(g-2)_\mu$ from the $e^+e^- \rightarrow K\bar{K}$ process comes from ϕ -meson energy region. The CMD-3 collaboration has studied both charge modes of this reaction, $K_S K_L$ and $K^+ K^-$.

The measured $e^+e^- \rightarrow K_S K_L$ cross section [13] is shown in Fig. 5 (left). From the fit to the cross section, the product of ϕ -meson parameters is extracted to be $B(\phi \rightarrow K_S K_L)\Gamma(\phi \rightarrow e^+e^-) =$

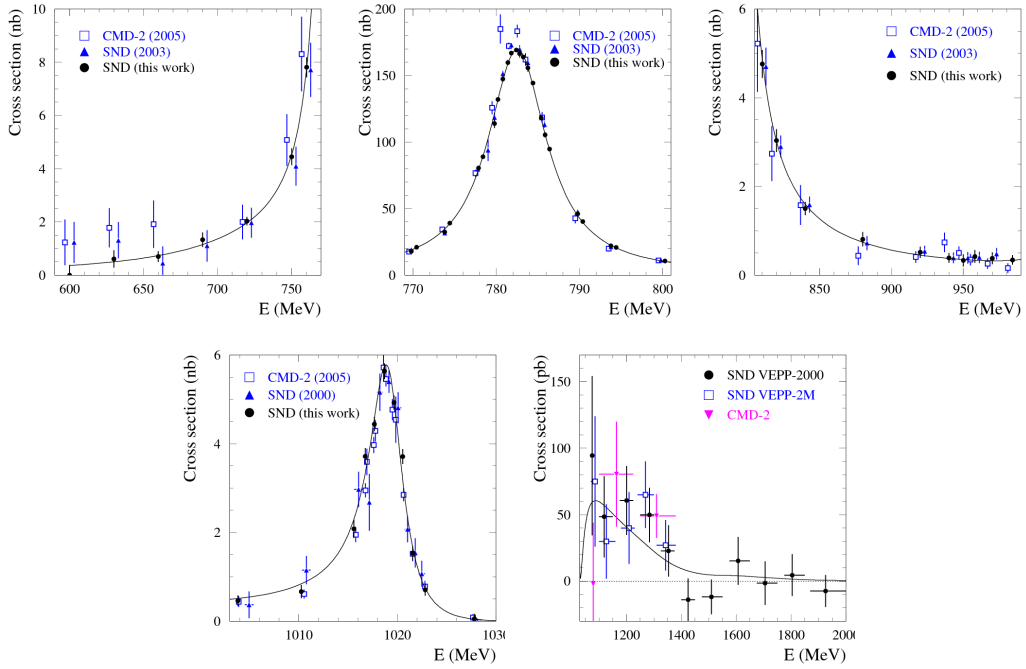


Figure 4: The $e^+e^- \rightarrow \pi^0\gamma$ cross section measured by SND using the full VEPP-2M data sample in comparison with the previous most accurate measurements. The curve is the result of the VMD fit. Only statistical errors are shown. The systematic errors are 3.2%, 3%, and 6% for SND (2000), SND (2003), and CMD-2 (2005) data, respectively. The systematic uncertainty of the current measurement at the ω and ϕ peaks is 1.4%. In the highest energy region the preliminary SND result based on VEPP2000 data is shown.

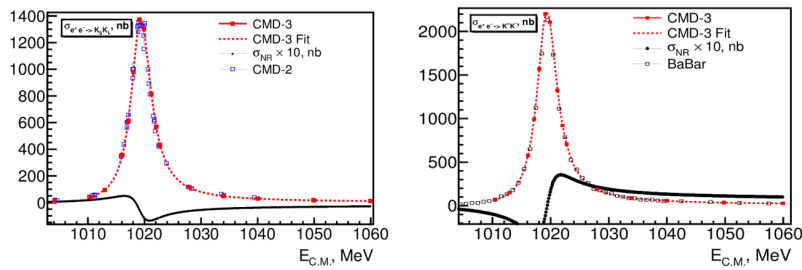


Figure 5: Left panel: The $e^+e^- \rightarrow K_S K_L$ cross section measured by CMD-3. Right panel: The $e^+e^- \rightarrow K^+ K^-$ cross section measured by CMD-3. In both plots the dotted curves are the results of the fit with the vector-meson dominance model including ρ , ω , ϕ and their excitations. The curves σ_{NR} represent the contributions to the cross sections corresponding interference between the ϕ -meson amplitude and the amplitudes of other vector mesons.

POS(FPSCP2017)029

428 ± 9 eV, which is in good agreement with the current PDG value 430 ± 6 eV [14]. The preliminary CMD-3 result on the e⁺e⁻ → K⁺K⁻ cross section is presented in Fig. 5 (right). From the fit to the cross section the product B(ϕ → K⁺K⁻)Γ(ϕ → e⁺e⁻) = 671 ± 20 eV is obtained, which is about 10% larger than the PDG2014 value 608 ± 14 eV based on the CMD-2 measurement at VEPP-2M and about 5% (1.7σ) larger than the recent BABAR result 634 ± 8 [15]. It should be noted that the CMD-3 ratio of decay constants for ϕ → K_SK_L and ϕ → K⁺K⁻ decays corrected for the Coulomb K⁺K⁻ final state interaction (0.990 ± 0.017) is close to unity expected from the isospin relations.

Figure 6 (left) represents the SND measurement of the e⁺e⁻ → K⁺K⁻ cross section in the energy range 1.05–2.00 GeV [16] in comparison with the most precise previous measurement by BABAR [15]. The SND results agree with BABAR data and have comparable or better accuracy. The right plot in Fig. 6 shows the ratio of the BABAR data to the fit to the SND data. The bands

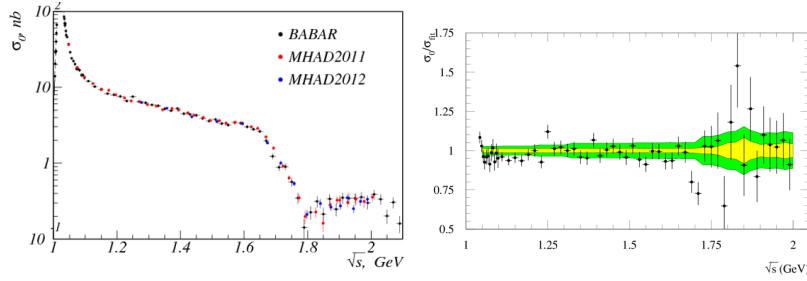


Figure 6: Left panel: The e⁺e⁻ → K⁺K⁻ cross section measured by SND at VEPP2000 and in the BABAR experiment. Right panel: The relative difference between the e⁺e⁻ → K⁺K⁻ cross sections measured by BABAR and the fit to the SND data. The SND and BABAR systematic uncertainties are shown by the light and dark shaded bands, respectively.

represent systematic uncertainties.

6. e⁺e⁻ → K \bar{K} π and e⁺e⁻ → K \bar{K} ππ

The exclusive data are incomplete in the region 1.6 < E < 2.0 GeV. There is no experimental information on the final states π⁺π⁻π⁰η, π⁺π⁻ηη, π⁺π⁻π⁰π⁰π⁰, π⁺π⁻π⁰π⁰η etc. The important experimental task is to measure all significant exclusive channels below 2 GeV, and perform comparison of the sum of exclusive channels with inclusive measurements and pQCD prediction. In this and the next two sections we discuss previously unmeasured processes giving sizable contribution into the total cross section between 1.6 and 2 GeV.

The reactions e⁺e⁻ → K_SK_Lπ⁰ is measured by BABAR for the first time [17]. The obtained cross section is shown in Fig. 7(left). Only statistical errors are shown. The systematic uncertainty is 10% near the cross-section peak and increases up to 30% at 3.0 GeV. The dominant intermediate state (more than 95% events) in this reaction is K*(892)K. The K₂*(1430)K and ϕπ⁰ intermediate states are also seen.

Two other charge combinations of the e⁺e⁻ → K \bar{K} π reaction were measured by BABAR previously [18]. So, we can calculate the total e⁺e⁻ → K \bar{K} π cross section without any assumptions about isospin relations between charge modes. The red points in Fig. 7(right) represent e⁺e⁻ →

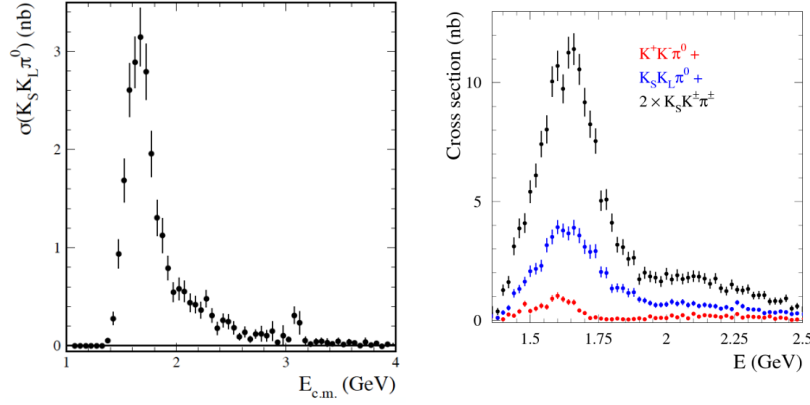


Figure 7: Left panel: The $e^+e^- \rightarrow K_S K_L \pi^0$ cross section measured by BABAR. Right panel: The total $e^+e^- \rightarrow K\bar{K}\pi$ cross section obtained as a sum of the cross sections measured in three charge modes: $\sigma(K_S K_L \pi^0) + \sigma(K^+ K^- \pi^0) + 2\sigma(K_S K^\pm \pi^\mp)$. The red points represent $K^+ K^- \pi^0$ cross section. The blue points are the sum of $K^+ K^- \pi^0$ and $K_S K_L \pi^0$ final states.

$K^+ K^- \pi^0$ cross section, the blue points are the sum of the cross sections for $K^+ K^- \pi^0$ and $K_S K_L \pi^0$, and the black points are the sum of all three charge modes. The $e^+e^- \rightarrow K\bar{K}\pi$ cross section in the maximum is about 12% of the total hadronic cross section.

The process $e^+e^- \rightarrow K\bar{K}\pi\pi$ contains six charge combinations. Four of them, $K^+ K^- \pi^+ \pi^-$, $K^+ K^- \pi^0 \pi^0$, $K_S K_L \pi^+ \pi^-$, and $K_S K_S \pi^+ \pi^-$, were measured by BABAR previously [19, 20]. In Fig. 8 the first measurements of the cross sections for two last charge modes, $K_S K_L \pi^0 \pi^0$ [17] and $K_S K^\pm \pi^\mp \pi^0$ [21], performed by BABAR are presented. Only statistical errors are shown. The $K_S K_L \pi^0 \pi^0$ cross section is found to be relatively small and measured with a 25% uncertainty in the peak. The dominant intermediate state for this process is $K^* \bar{K} \pi$. The correlated production of two K^* 's is observed to be small. The $K_S K^+ \pi^- \pi^0$ cross section is measured with 6–7% uncertainty below 3 GeV. The dominant intermediate states for this reaction are $K^* \bar{K} \pi$ and $K_S K^\pm \rho^\mp$. The correlated $K^* \bar{K}^*$ production is small, less than 15%, and dominated by the charged mode, $K^{*+} \bar{K}^{*-}$.

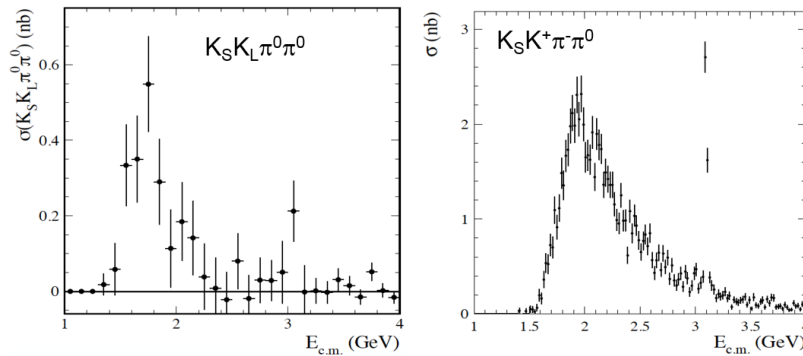


Figure 8: The $e^+e^- \rightarrow K_S K_L \pi^0 \pi^0$ (left) and $e^+e^- \rightarrow K_S K^\pm \pi^\mp \pi^0$ (right) cross sections measured by BABAR.

Figure 9 shows the cross sections for the six charge modes summed cumulatively. The black

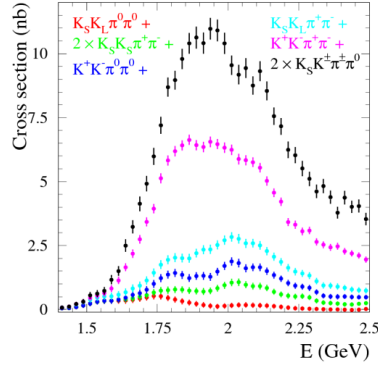


Figure 9: The cross sections for the six charge modes of the $e^+e^- \rightarrow K\bar{K}\pi\pi$ process summed cumulatively. The black points represent the total cross section.

points represent the total cross section. Largest contributions come from the $K^+K^-\pi^+\pi^-$ and $K_S K^+ \pi^-\pi^0$ modes. The $e^+e^- \rightarrow K\bar{K}\pi\pi$ cross section is about 25% of the total hadronic cross section near 2 GeV.

7. $e^+e^- \rightarrow \omega\pi^0\eta$

The process $e^+e^- \rightarrow \pi^0\pi^0\eta\gamma$ was studied by the SND detector in the seven-photon final state [22]. Events of the $e^+e^- \rightarrow \pi^0\pi^0\eta\gamma$ process are selected. The analysis of their $\pi^0\gamma$ invariant-mass distribution shows the dominance of the $\omega\pi^0\eta$ intermediate state. The measured $e^+e^- \rightarrow \omega\pi^0\eta$ cross section is shown in Fig. 10 (left). Figure 10 (right) shows the $\pi^0\eta$ mass distribution for selected $\omega\pi^0\eta$ events, which is well described by the model of the $\omega a_0(980)$ intermediate state.

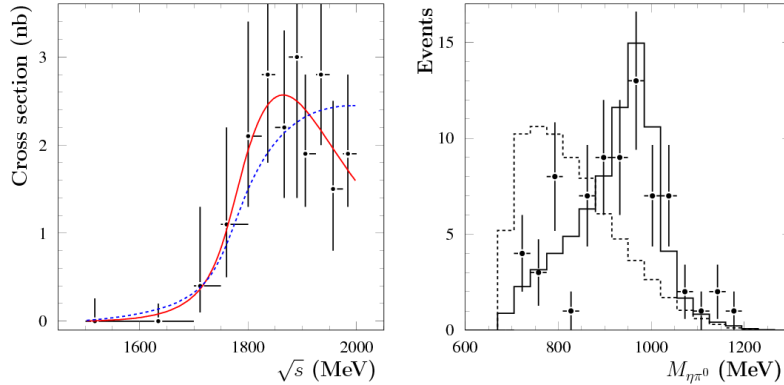


Figure 10: Left panel: The $e^+e^- \rightarrow \omega\eta\pi^0$ cross section measured by SND. The solid (dashed) curve shows the result of the fit in the model of $\omega a_0(980)$ intermediate state with (without) a resonance contribution. Right panel: The $\eta\pi^0$ invariant mass spectrum for selected $e^+e^- \rightarrow \omega\eta\pi^0$ events. The solid histogram represents $e^+e^- \rightarrow \omega a_0(980)$ simulation, while the dashed histogram represents $\omega\eta\pi^0$ phase-space simulation.

This previously unmeasured cross section is found to be relatively large, about 5% of the total hadronic cross section.

8. e⁺e⁻ → π⁺π⁻π⁰η

The SND detector also has studied the e⁺e⁻ → π⁺π⁻π⁰η process. It has complex internal structure. There are at least four mechanisms for this reaction: ωη, φη, a₀(980)ρ, and structureless π⁺π⁻π⁰η. The known ωη and φη contributions explain about 50-60% of the cross section below 1.8 GeV. Above 1.8 GeV the dominant mechanism is a₀ρ. The preliminary result on the e⁺e⁻ → π⁺π⁻π⁰η cross section is shown in Fig. 11 (left). The cross section for the subprocess e⁺e⁻ → ωη is measured separately [23] and shown in Fig. 11 (right) in comparison with the BABAR measurement [24]. The SND results have better accuracy and disagree with the BABAR data at E > 1.6 GeV.

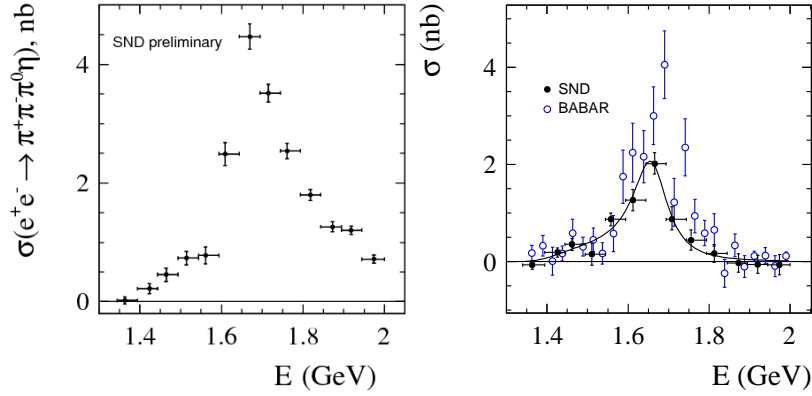


Figure 11: Left panel: The e⁺e⁻ → π⁺π⁻π⁰η cross section measured by SND. Right panel: The e⁺e⁻ → ωη cross section measured by SND in comparison with BABAR data [24]. The curve is the result of the VMD fit.

9. Summary

The precise low-energy e⁺e⁻ cross section data are needed to obtain an accurate SM prediction for the muon anomalous magnetic moment.

Recent results on e⁺e⁻ → π⁺π⁻, π⁺π⁻π⁰π⁰, K⁺K⁻, K⁺K⁻π, K⁺K⁻ππ cross sections from BES III, BABAR, SND, CMD-2 and R measurement from KEDR [25, 26] are already taken into account in the recent calculations of a_μ^{had, LO} [4] and reduce its uncertainty.

Several previously unmeasured processes (e⁺e⁻ → K_SK_Lπ⁰, K_SK_Lπ⁰π⁰, K_SK[±]π[∓]π⁰, π⁺π⁻π⁻η, and ωπ⁰η) contributed to the total hadronic cross section below 2 GeV have been studied.

New results are expected from BESIII, BABAR, SND, CMD-3.

References

- [1] G. W. Bennett *et al.* (Muon g-2 Collaboration) Phys. Rev. D **73**, 072003 (2006).
- [2] J. Grange *et al.* (Muon g-2 Collaboration), arXiv:1501.06858 [physics.ins-det].
- [3] M. Otani (E34 Collaboration), JPS Conf. Proc. **8**, 025008 (2015).
- [4] M. Davier, A. Hoecker, B. Malaescu and Z. Zhang, arXiv:1706.09436 [hep-ph].

- [5] F. Jegerlehner, arXiv:1705.00263 [hep-ph].
- [6] R. R. Akhmetshin *et al.* (CMD-2 Collaboration), Phys. Lett. B **578**, 285 (2004); V. M. Aulchenko *et al.* (CMD-2 Collaboration), JETP Lett. **82**, 743 (2005); R. R. Akhmetshin *et al.* (CMD-2 Collaboration), JETP Lett. **84**, 413 (2006); R. R. Akhmetshin *et al.* (CMD-2 Collaboration), Phys. Lett. B **648**, 28 (2007).
- [7] A. Aloisio *et al.* (KLOE Collaboration), Phys. Lett. B **606**, 12 (2005); F. Ambrosino *et al.* (KLOE Collaboration), Phys. Lett. B **670**, 285 (2009); F. Ambrosino *et al.* (KLOE Collaboration), Phys. Lett. B **700**, 102 (2011); D. Babusci *et al.* [KLOE Collaboration], Phys. Lett. B **720**, 336 (2013).
- [8] B. Aubert *et al.* (BaBar Collaboration), Phys. Rev. Lett. **103**, 231801 (2009).
- [9] M. Ablikim *et al.* (BESIII Collaboration), Phys. Lett. B **753**, 629 (2016).
- [10] M. Davier, A. Hoecker, B. Malaescu and Z. Zhang, Eur. Phys. J. C **71**, 1515 (2011); Erratum: [Eur. Phys. J. C **72**, 1874 (2012)].
- [11] V. P. Druzhinin, arXiv:0710.3455 [hep-ex].
- [12] M. N. Achasov *et al.* (SND Collaboration), Phys. Rev. D **93**, 092001 (2016).
- [13] E. A. Kozyrev *et al.* (CMD-3 Collaboration), Phys. Lett. B **760**, 314 (2016).
- [14] C. Patrignani *et al.* (Particle Data Group), Chin. Phys. C, **40**, 100001 (2016).
- [15] J. P. Lees *et al.* (BaBar Collaboration), Phys. Rev. D **88**, 032013 (2013).
- [16] M. N. Achasov *et al.* (SND Collaboration), Phys. Rev. D **94**, 112006 (2016).
- [17] J. P. Lees *et al.* (BABAR Collaboration), Phys. Rev. D **95**, 052001 (2017).
- [18] B. Aubert *et al.* (BABAR Collaboration), Phys. Rev. D **77**, 092002 (2008).
- [19] J. P. Lees *et al.* (BABAR Collaboration), Phys. Rev. D **86**, 012008 (2012).
- [20] J. P. Lees *et al.* (BABAR Collaboration), Phys. Rev. D **89**, 092002 (2014).
- [21] J. P. Lees *et al.* (BABAR Collaboration), Phys. Rev. D **95**, 092005 (2017).
- [22] M. N. Achasov *et al.* (SND Collaboration), Phys. Rev. D **94**, 032010 (2016).
- [23] M. N. Achasov *et al.* (SND Collaboration), Phys. Rev. D **94**, 092002 (2016).
- [24] B. Aubert *et al.* (BABAR Collaboration), Phys. Rev. D **73**, 052003 (2006).
- [25] V. V. Anashin *et al.* (KEDR Collaboration), Phys. Lett. B **753**, 533 (2016).
- [26] V. V. Anashin *et al.* (KEDR Collaboration), Phys. Lett. B **770**, 174 (2017).